

Title	High energy radiation from jets and accretion disks near rotating black holes
Authors	O'Riordan, Michael;Pe'er, Asaf;McKinney, Jonathan C.
Publication date	2017-01
Original Citation	O'Riordan, M., Pe'er, A. and McKinney, J.C. (2017) 'High energy radiation from jets and accretion disks near rotating black holes', AIP Conference Proceedings 1792, 040042, (6pp). doi: 10.1063/1.4968946
Type of publication	Conference item
Link to publisher's version	10.1063/1.4968946
Rights	© 2017, the Authors. Reproduced with the permission of AIP Publishing from AIP Conference Proceedings 1792, 040042 (2017); doi: 10.1063/1.4968946
Download date	2025-08-14 09:59:14
Item downloaded from	https://hdl.handle.net/10468/3952

High energy radiation from jets and accretion disks near rotating black holes

Michael O’Riordan, Asaf Pe’er, and Jonathan C. McKinney

Citation: **1792**, 040042 (2017); doi: 10.1063/1.4968946

View online: <http://dx.doi.org/10.1063/1.4968946>

View Table of Contents: <http://aip.scitation.org/toc/apc/1792/1>

Published by the [American Institute of Physics](#)

High Energy Radiation From Jets and Accretion Disks Near Rotating Black Holes

Michael O' Riordan^{1,a)}, Asaf Pe'er¹ and Jonathan C. McKinney²

¹*Physics Department, University College Cork, Cork, Ireland*

²*Department of Physics and Joint Space-Science Institute, University of Maryland, College Park, MD 20742, USA*

^{a)}michael.oriordan@umail.ucc.ie

Abstract. We model the low/hard state in X-ray binaries as a magnetically arrested accretion flow, and calculate the resulting radiation using a general-relativistic radiative transport code. Firstly, we investigate the origin of the high-energy emission. We find the following indications of a significant jet contribution at high energies: (i) a pronounced γ -ray peak at $\sim 10^{23}$ Hz, (ii) a break in the optical/UV band where the spectrum changes from disk to jet dominated, and (iii) a low-frequency synchrotron peak $\lesssim 10^{14}$ Hz implies that a significant fraction of any observed X-ray and γ -ray emission originates in the jet. Secondly, we investigate the effects of black hole spin on the high-energy emission. We find that the X-ray and γ -ray power depend strongly on spin and inclination angle. Surprisingly, this dependence is not a result of the Blandford-Znajek mechanism, but instead can be understood as a redshift effect. For rapidly rotating black holes, observers with large inclinations see deeper into the hot, dense, highly-magnetized inner regions of the accretion flow. Since the lower frequency emission originates at larger radii, it is not significantly affected by the spin. Therefore, the ratio of the X-ray to near-infrared power is an observational probe of black hole spin.

Introduction

Jets exist in a wide range of accreting black hole systems, from stellar mass black holes in X-ray binaries (XRBs), to supermassive black holes in active galactic nuclei. While it is generally accepted that jets are responsible for the observed radio emission [e.g., 1], their contribution to the high-energy (X-ray and γ -ray) radiation is less certain. In particular, although the X-ray emission in XRBs has long been modelled as inverse Compton scattering from a corona of hot electrons surrounding the inner accretion disk [e.g., 2–10], it is also possible that this emission is produced by jets [e.g., 11–17].

Narayan and McClintock [18] found a correlation between 5 GHz radio emission from XRBs and black hole spin. Assuming that this emission can be used as a proxy for the jet power, their results were consistent with $P_{\text{jet}} \sim a^2$, which is the scaling derived by Blandford and Znajek [19]. Therefore, if confirmed, their results provide observational support for jet launching via the Blandford-Znajek (BZ) mechanism. That is, jets are driven by the rotational energy of black holes. However, since the high-energy emission could originate from much closer to the black hole, it is not clear whether this radiation should follow the same correlation as the radio emission. In this work, we examine the radiation resulting from the complicated interaction between the inner disk/jet and central black hole.

Radiatively inefficient advection-dominated accretion flows (ADAFs) have been used extensively to model low luminosity systems with $L \ll L_{\text{Edd}}$, where L_{Edd} is the Eddington luminosity [7, 20]. We model the low/hard state in XRBs as an ADAF in the so-called “magnetically arrested disk” (MAD) state [21]. We use fully 3D general-relativistic magnetohydrodynamic (GRMHD) simulations of MADs from [22, 23], which show efficient extraction of black hole rotational energy via the BZ mechanism.

We calculate spectra using a radiative transport code based on the freely available grmonty [24]. We consider synchrotron emission, self-absorption, and Compton scattering from a thermal distribution of relativistic electrons. For simplicity, we assume that the electron temperature is a constant fraction of the proton temperature. The density and magnetization can vary significantly between the disk and jet, leading to different cooling rates in these regions [25, 26]. Therefore, we allow the proton-to-electron temperature ratio $\mathcal{T} \equiv T_p/T_e$ to vary independently in the disk and jet, which we denote by \mathcal{T}_d and \mathcal{T}_j , respectively.

In the following sections, we present the results of our investigations of the observational signatures of jet emission [17], and the effects of black hole spin on the high-energy radiation [27]. For the purpose of studying jet signatures, we consider the fiducial model, A0.94BfN40, from [23]. This model has spin of $a = 0.9375$, and launches a Poynting flux dominated jet with efficiency (defined as the energy extracted versus energy lost to the black hole) reaching $> 300\%$. For our investigation of the effects of black hole spin, we choose five models with spins $a = \{0.1, 0.2, 0.5, 0.9, 0.99\}$, corresponding to A0.1N100, A0.2N100, A0.5N100, A0.9N100, and A0.99N100 from [23].

Jet Signatures

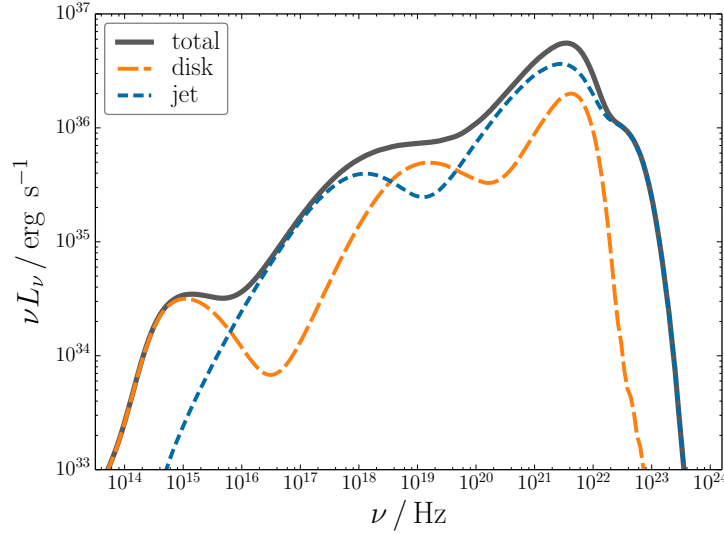


FIGURE 1. Spectrum for MAD model with $\mathcal{T}_d = \mathcal{T}_j = 10$. The long dashed line shows the contribution from the disk and the short dashed line shows the contribution from the jet. In this case, the disk mainly dominates in the optical/UV band, while the jet dominates the X-rays and γ -rays. There is significant γ -ray emission at $\sim 10^{23}$ Hz, produced by scattering from hot electrons in the jet. There is also a clear spectral break at $\sim 10^{16}$ Hz, above which the emission is primarily dominated by the jet. This spectral break results from the overlapping disk and jet components. Adapted from [17].

In Figure 1 we show the spectrum calculated with $\mathcal{T}_d = \mathcal{T}_j = 10$. The solid line shows the composite spectrum, while the contributions from the jet and disk are defined as follows. The disk (long dashes) component corresponds to photons which originated in the disk and escaped without interacting with the jet. The jet (short dashes) component shows the contribution from photons which either originated in the jet, or were re-processed by the jet before escaping.

In this case, the X-rays and γ -rays are mainly dominated by the jet, while the disk contributes significantly in the optical/UV band. The peaks at $\sim 10^{15}$ Hz and $\sim 10^{18}$ Hz are due to synchrotron emission from the disk and jet, respectively. The higher energy spectral features result from either single or double Compton scattering. The peaks in the disk component at $\sim 10^{19}$ Hz and $\sim 10^{22}$ Hz result from single and double scattering of synchrotron photons which originated in the disk. The peak in the jet component at $\sim 10^{23}$ Hz is due to scattering from hot electrons in the jet, while the peak at $\sim 10^{22}$ Hz results from photons which originated in the jet and scattered once in the disk before escaping. There is also a clear break in the spectrum at $\sim 10^{16}$ Hz, with a change from $\nu L_\nu \sim \nu^0$ to $\nu L_\nu \sim \nu$. This break results from the overlapping disk and jet components, and is located where the spectrum changes from disk to jet dominated.

In Figure 2 we show the effects of varying the jet proton-to-electron temperature ratio \mathcal{T}_j . This parameter adjusts the relative contribution from the jet. In the left panel we show the case with $\mathcal{T}_d = 10$ and $\mathcal{T}_j = 3$. Clearly, the jet dominates at all frequencies above $\sim 10^{16}$ Hz. As in Figure 1, there is a pronounced γ -ray peak at $\sim 10^{23}$ Hz, as well as a break at $\sim 10^{16}$ Hz. The right panel shows $\mathcal{T}_d = 10$ and $\mathcal{T}_j = 30$. Here, the jet is sub-dominant and the features

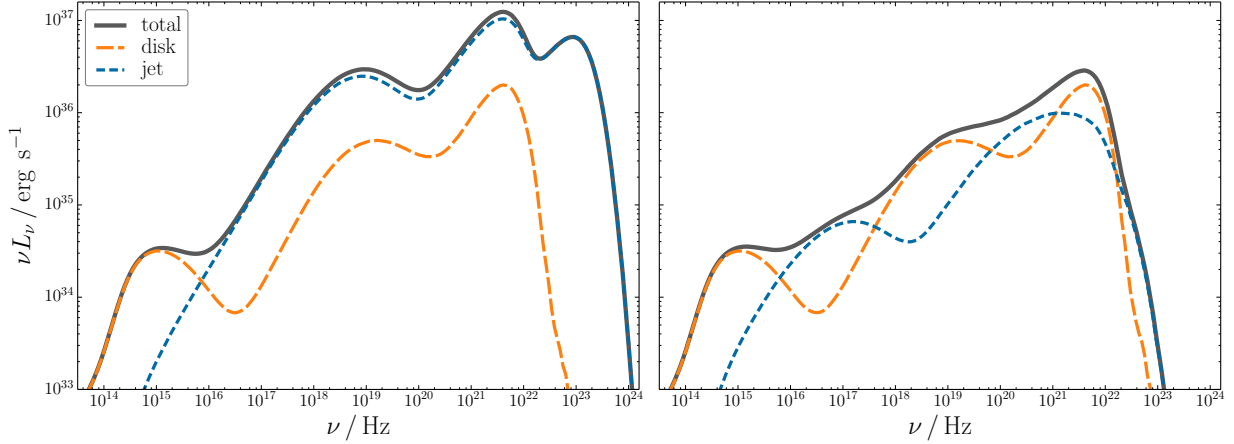


FIGURE 2. Spectra showing the effects of varying the relative jet contribution via the temperature ratio \mathcal{T}_j . As in Figure 1, both panels have $\mathcal{T}_d = 10$. The left panel has $\mathcal{T}_j = 3$, and the right panel has $\mathcal{T}_j = 30$. The spectrum in the left panel is strongly jet dominated and shows a significant peak in the γ -rays at $\sim 10^{23}$ Hz, as well as a break in the spectrum at $\sim 10^{16}$ Hz. In the right panel, the jet is sub-dominant and these features are absent or obscured by the disk emission. Adapted from [17].

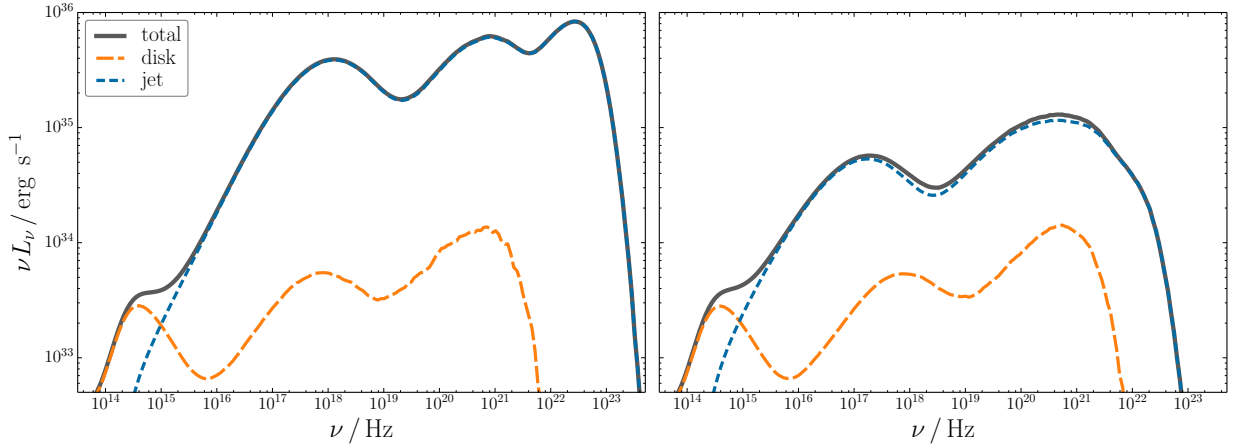


FIGURE 3. Spectra showing a larger disk temperature ratio of $\mathcal{T}_d = 30$. The left panel has $\mathcal{T}_j = 10$, and the right panel has $\mathcal{T}_j = 30$. In this case, the disk emission peaks just above $\sim 10^{14}$ Hz, while the X-rays and γ -rays are completely dominated by the jet. Adapted from [17].

apparent in the previous spectra are absent. Therefore, we conclude that these spectral features are signatures of jet emission.

In Figure 3 we increase the temperature ratio in the disk to $\mathcal{T}_d = 30$. In this case, the spectra are jet dominated at most frequencies, for a wide range of \mathcal{T}_j . The contribution from the disk is limited to frequencies below $\sim 10^{15}$ Hz, with the peak of the synchrotron emission located just above $\sim 10^{14}$ Hz. This implies that if the disk emission peaks at frequencies $\lesssim 10^{14}$ Hz, any observed X-ray and γ -ray emission likely originates in the jet.

Radiated Power vs Spin

In the left panel of Figure 4 we show the time-averaged, frequency-integrated radiated power for different spins and viewing angles. For comparison, the dashed line shows the scaling expected if the spin-dependence results from the BZ mechanism. The radiated power in our models clearly deviates significantly from this. In particular, for observers

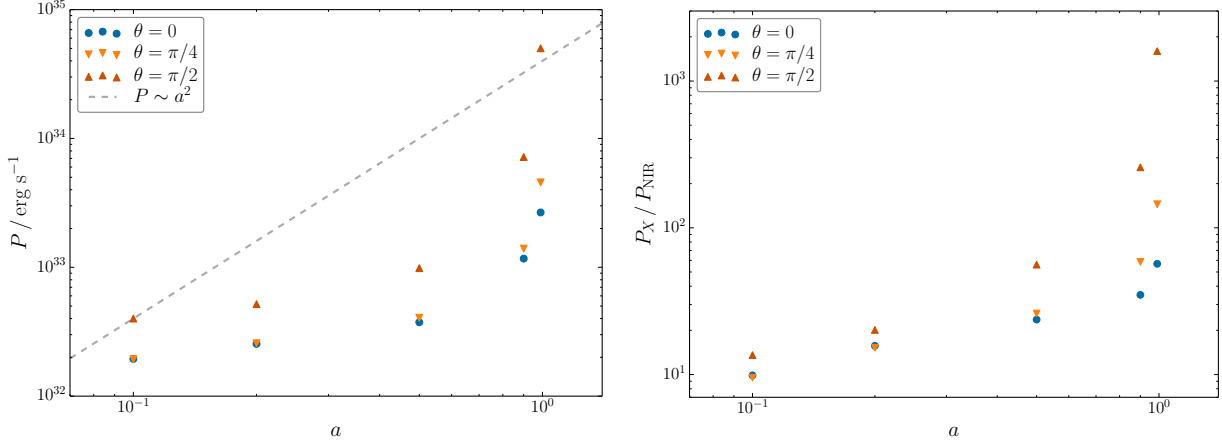


FIGURE 4. The left panel shows the observed frequency-integrated power vs spin for different observer inclinations. The radiated power increases with spin and clearly deviates significantly from a simple power law. For comparison, the dashed line shows the BZ scaling $P \sim a^2$. Furthermore, observed power reaches a maximum for observers located perpendicular to the spin axis. The right panel shows the ratio of the X-ray power to the NIR power as a function of spin and observer inclination angles. For large inclinations, this ratio increases dramatically with spin. Adapted from [27].

with $\theta = \pi/2$, there is an increase of nearly an order of magnitude between the $a = 0.9$ and $a = 0.99$ cases. As we explain below, the emission in our models is dominated by the near horizon region, and the spin and viewing angle dependence is a direct result of the strong gravitational redshift experienced by the photons.

In the right panel of Figure 4 we show the ratio of the observed X-ray to near-infrared (NIR) power P_X/P_{NIR} . As with the frequency-integrated power, this quantity strongly depends on both spin and observer inclination. This frequency dependence is a simple consequence of the location of emission. The X-rays originate closer to the black hole than the NIR emission and so are more sensitive to the strong gravitational effects. We conclude that, for systems whose inclination angles are known, the ratio P_X/P_{NIR} could potentially be used as a probe of black hole spin in the low/hard state.

To understand the results in Figure 4, we must consider the strong gravitational effects in the near horizon region. In particular, for a photon 4-momentum p^μ , and fluid 4-velocity u^μ , we define the redshift \mathcal{R} to be the ratio of the energy at infinity to the energy in the comoving frame

$$\mathcal{R} = \frac{E_\infty}{E} = \frac{\xi^\mu p_\mu}{u^\mu p_\mu} = \frac{p_t}{u^\mu p_\mu} \quad (1)$$

Here, ξ^μ is the Killing vector associated with stationarity. In the last equality we have specialised to Boyer-Lindquist coordinates, setting $\xi^\mu = \delta_t^\mu$. In the left panels of Figure 5 we show the redshift profiles calculated numerically for different spins and viewing angles (a) : $\theta = 0$, (b) : $\theta = \pi/2$. Interestingly, for high spins and inclinations, photons suffer little net redshift until very close to the horizon. This is the origin of the strong dependence on spin and viewing angle presented in Figure 4. That is, observers with $\theta = \pi/2$ see deeper into the hot, dense, highly-magnetized inner regions of the accretion flow.

In the right panels of Figure 5 we show the spectra for different spins and observer inclinations. The top panel shows spectra for $\theta = \pi/2$, which maximizes the deviations due to spin. As with the total radiated power, the frequency of the peak emission also increases significantly with spin. Since the NIR emission originates at larger radii, it is roughly constant with spin, while the X-rays and γ -rays, which originate much closer to the horizon, vary substantially. The bottom right panel shows the effects of viewing angle in the $a = 0.9$ case. Although there is little difference between the $\theta = 0$ and $\theta = \pi/4$ cases, the peak luminosity increases by nearly an order of magnitude between $\theta = \pi/4$ and $\theta = \pi/2$. Therefore, for large observer inclinations, we expect the ratio P_X/P_{NIR} to be extremely sensitive to the black hole spin.

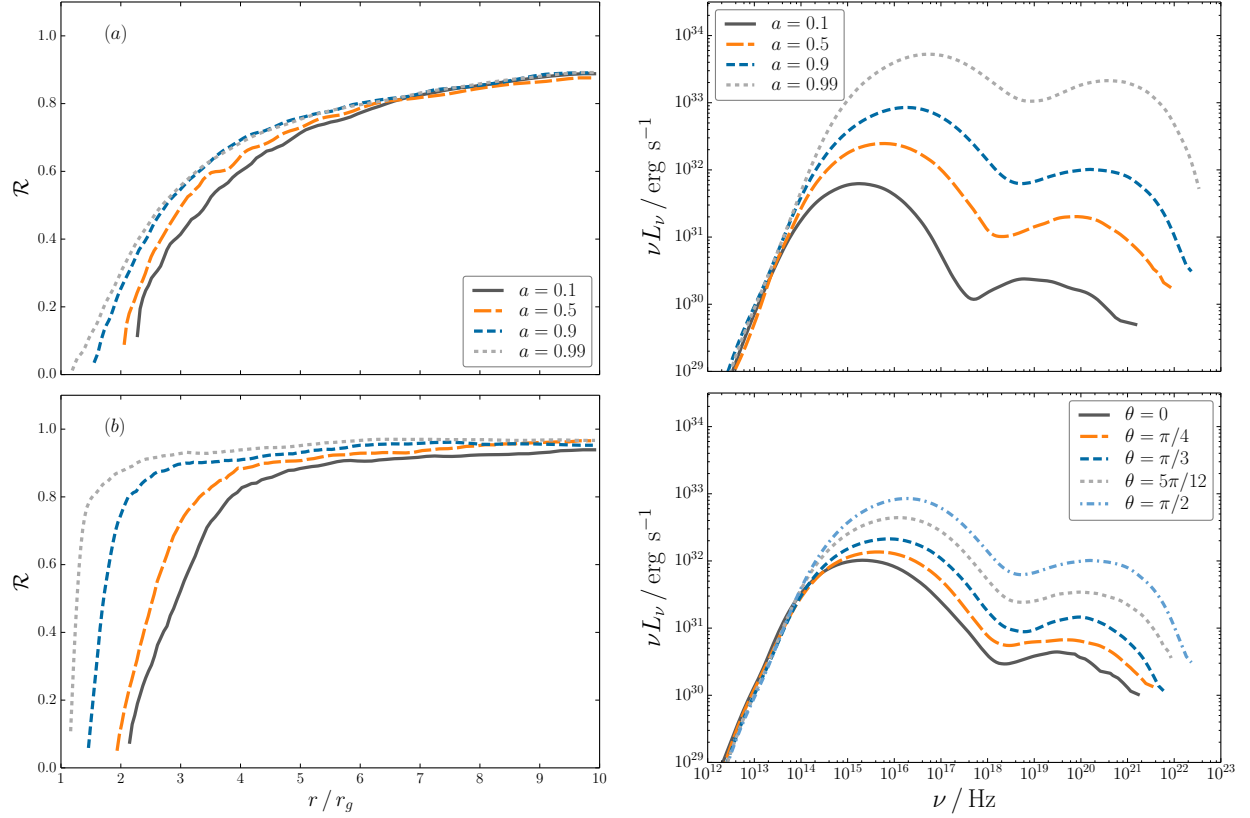


FIGURE 5. The left panels show the numerically calculated redshift profiles for different spins and observer inclinations (a) : $\theta = 0$, (b) : $\theta = \pi/2$. Photons received by observers with $\theta = \pi/2$ suffer little net redshift until originating from very close to the horizon. Such observers see deeper into the inner accretion flow than observers with $\theta = 0$. The top right panel shows the effects of spin on the spectra for observers with $\theta = \pi/2$. The X-rays and γ -rays come from close to the horizon and vary significantly with spin. The NIR emission originates further from the black hole and so is less sensitive to the spacetime geometry. The bottom right panel shows the effects of observer inclination in the $a = 0.9$ case. Adapted from [27].

Summary

In this work, we calculated the spectra of MADs in the context of the low/hard state in XRBs. In particular, we investigated the observational signatures of jet emission, as well as the effects of black hole spin and observer inclination on the high-energy radiation. We identified the following signatures of a significant jet contribution to the observed emission: (i) a pronounced peak in the γ -rays at $\sim 10^{23}$ Hz, (ii) a break in the optical/UV band resulting from the overlapping disk and jet components, and (iii) a synchrotron peak near or below $\sim 10^{14}$ Hz implies that any observed X-ray and γ -ray emission is produced by the jet.

We found that the high-energy power depends strongly on both black hole spin and observer inclination. Interestingly, this is not a consequence of the BZ mechanism, but instead can be understood as a redshift effect. For high spins and viewing angles, photons suffer little net redshift until originating from very close to the horizon. Therefore, observers with $\theta \sim \pi/2$ receive photons from a region with very high density, electron temperature, and magnetization. Furthermore, since the lower-frequency emission originates at larger radii, it is less sensitive to the spacetime geometry. This introduces a significant frequency dependence which can be used to probe the black hole spin. We identified the ratio of the X-ray to NIR luminosity as a potential observational signature of spin in the low/hard state.

Acknowledgements

JCM would like to thank Alexander Tchekhovskoy for providing simulation data. MOR is supported by the Irish Research Council under grant number GOIPG/2013/315. This research was partially supported by the European Union Seventh Framework Programme (FP7/2007-2013) under grant agreement no 618499. JCM acknowledges NASA/NSF/TCAN (NNX14AB46G), NSF/XSEDE/TACC (TGPHY120005), and NASA/Pleiades (SMD-14-5451).

REFERENCES

- [1] R. Fender, “‘Disc-Jet’ Coupling in Black Hole X-Ray Binaries and Active Galactic Nuclei,” in *Lecture Notes in Physics, Berlin Springer Verlag*, [Lecture Notes in Physics, Berlin Springer Verlag](#), Vol. 794, edited by T. Belloni (2010) p. 115, arXiv:0909.2572 [astro-ph.HE] .
- [2] P. Magdziarz and A. A. Zdziarski, *MNRAS* **273**, 837–848 (1995).
- [3] M. Gierlinski, A. A. Zdziarski, C. Done, W. N. Johnson, K. Ebisawa, Y. Ueda, F. Haardt, and B. F. Phlips, *MNRAS* **288**, 958–964 (1997), arXiv:astro-ph/9610156 .
- [4] A. A. Esin, J. E. McClintock, and R. Narayan, *ApJ* **489**, 865–889 (1997), arXiv:astro-ph/9705237 .
- [5] A. A. Esin, J. E. McClintock, J. J. Drake, M. R. Garcia, C. A. Haswell, R. I. Hynes, and M. P. Muno, *ApJ* **555**, 483–488 (2001), arXiv:astro-ph/0103044 .
- [6] F. Yuan, A. A. Zdziarski, Y. Xue, and X.-B. Wu, *ApJ* **659**, 541–548 (2007), arXiv:astro-ph/0608552 .
- [7] R. Narayan and J. E. McClintock, *NewAR* **51**, 733–751 (2008), arXiv:0803.0322 .
- [8] A. Niedźwiecki, F.-G. Xie, and A. A. Zdziarski, *MNRAS* **420**, 1195–1206 (2012), arXiv:1107.0860 [astro-ph.HE] .
- [9] A. Niedźwiecki, F.-G. Xie, and A. Stępnik, *MNRAS* **443**, 1733–1747 (2014), arXiv:1406.6003 [astro-ph.HE] .
- [10] E. Qiao and B. F. Liu, *MNRAS* **448**, 1099–1106 (2015), arXiv:1501.03565 [astro-ph.HE] .
- [11] S. Markoff, H. Falcke, and R. Fender, *A&A* **372**, L25–L28 (2001), [arXiv:astro-ph/0010560](#) .
- [12] S. Markoff, M. Nowak, S. Corbel, R. Fender, and H. Falcke, *A&A* **397**, 645–658 (2003), [arXiv:astro-ph/0210439](#) .
- [13] S. Markoff, M. A. Nowak, and J. Wilms, *ApJ* **635**, 1203–1216 (2005), arXiv:astro-ph/0509028 .
- [14] A. Pe’er and P. Casella, *ApJ* **699**, 1919–1937 (2009), arXiv:0902.2892 [astro-ph.HE] .
- [15] A. Pe’er and S. Markoff, *ApJ* **753**, p. 177 (2012), arXiv:1105.4896 [astro-ph.HE] .
- [16] S. Markoff, M. Nowak, E. Gallo, R. Hynes, J. Wilms, R. M. Plotkin, D. Maitra, C. V. Silva, and S. Drappeau, *ArXiv e-prints* (2015), [arXiv:1510.02244](#) [astro-ph.HE] .
- [17] M. O’ Riordan, A. Pe’er, and J. C. McKinney, *ApJ* **819**, p. 95 (2016), arXiv:1510.08860 [astro-ph.HE] .
- [18] R. Narayan and J. E. McClintock, *MNRAS* **419**, L69–L73 (2012), arXiv:1112.0569 [astro-ph.HE] .
- [19] R. D. Blandford and R. L. Znajek, *MNRAS* **179**, 433–456 (1977).
- [20] F. Yuan and R. Narayan, *ARA&A* **52**, 529–588 (2014), arXiv:1401.0586 [astro-ph.HE] .
- [21] R. Narayan, I. V. Igumenshchev, and M. A. Abramowicz, *PASJ* **55**, L69–L72 (2003), astro-ph/0305029 .
- [22] A. Tchekhovskoy, R. Narayan, and J. C. McKinney, *MNRAS* **418**, L79–L83 (2011), arXiv:1108.0412 [astro-ph.HE] .
- [23] J. C. McKinney, A. Tchekhovskoy, and R. D. Blandford, *MNRAS* **423**, 3083–3117 (2012), arXiv:1201.4163 [astro-ph.HE] .
- [24] J. C. Dolence, C. F. Gammie, M. Mościbrodzka, and P. K. Leung, *ApJS* **184**, 387–397 (2009).
- [25] S. M. Ressler, A. Tchekhovskoy, E. Quataert, M. Chandra, and C. F. Gammie, *MNRAS* **454**, 1848–1870 (2015), arXiv:1509.04717 [astro-ph.HE] .
- [26] F. Foucart, M. Chandra, C. F. Gammie, and E. Quataert, *MNRAS* **456**, 1332–1345 (2016), arXiv:1511.04445 [astro-ph.HE] .
- [27] M. O’ Riordan, A. Pe’er, and J. C. McKinney, *ArXiv e-prints* (2016), [arXiv:1607.01060](#) [astro-ph.HE] .